Available online at www.sciencedirect.com

ScienceDirect

IFAC Papers Online CONFERENCE PAPER ARCHIVE

IFAC-PapersOnLine 49-17 (2016) 338–342

Nonlinear Dynamic Inversion of a Flexible Aircraft

Ryan James Caverly * **Anouck R. Girard** *
Ilya V. Kolmanovsky * **James Richard Forbes** **

* *Department of Aerospace Engineering, University of Michigan, 1320 Beal Avenue, Ann Arbor, MI 48109, USA (emails: caverly@umich.edu, anouck@umich.edu, ilya@umich.edu.)*
** *Department of Mechanical Engineering, McGill University, 817 Sherbrooke Street West, Montreal, Quebec, Canada H3A 0C3 (email: james.richard.forbes@mcgill.ca)*

Abstract: This paper investigates the use of dynamic inversion for the attitude control of a flexible aircraft. Input-output feedback linearization-based dynamic inversion is used to linearize the angular velocity and forward translational velocity equations of motion. A proportional-integral-derivative (PID) controller based on the direction cosine matrix (DCM) that describes the attitude of the aircraft is used, in addition to a proportional-integral (PI) controller to maintain a desired airspeed. Numerical simulations are performed using the proposed dynamic inversion controller, as well as more practical implementations of the controller that include saturated control inputs and no knowledge of the aircraft's flexible states. In simulation, the practical controllers successfully stabilize a flexible aircraft with reasonable control surface deflections.

Keywords: Dynamic inversion, feedback linearization, aircraft control, saturation control, PID control, flexible wings.

1. INTRODUCTION

Dynamic inversion has been shown to be an efficient control method for aircraft, due to its ability to transform nonlinear equations of motion into linear equations over large operating regimes (Enns et al., 1994). Dynamic inversion is a nonlinear control technique that is equivalent to input-output feedback linearization (Sastry and Isidori, 1989; Hovakimyan et al., 2005). As the performance limits of aircraft continue to expand, lighter and consequently more flexible aircraft are produced. This flexibility has been modeled (Tuzcu et al., 2007; Patil et al., 1999; Caverly and Forbes, 2015) and incorporated into the dynamic inversion control framework (Gregory, 2001; Dillsaver et al., 2013). However, the work of Gregory (2001) and Dillsaver et al. (2013) only consider the longitudinal dynamics of a flexible aircraft. There exists literature on the use of dynamic inversion for attitude control of flexible spacecraft (Tafazoli and Khorasani, 2004; Malekzadeh et al., 2010), which contains techniques that can be used as inspiration for the dynamic inversion of a flexible aircraft.

The novel contribution of this work includes the design and analysis of a controller that employs dynamic inversion for attitude and airspeed control of flexible aircraft. In particular, the use of dynamic inversion with practical constraints on the number of measured states and on the magnitude of the control inputs is considered. As proposed in Tafazoli and Khorasani (2004), dynamic inversion of the angular velocity equation of motion is performed. The dynamic inversion presented in this paper differs from that in Tafazoli and Khorasani (2004) by the inclusion of the aircraft's forward velocity in the dynamic inversion process, which allows for the linearization of the aircraft's angular velocity and forward velocity equations of motion. A proportional-integral-derivative attitude control law based on the direction cosine matrix (DCM) is considered along with a proportional-integral (PI) control law for airspeed control. The proposed dynamic inversion controller is implemented in simulation on a flexible high-altitude long-endurance (HALE) aircraft. More practical forms of the proposed controller are also implemented, which include limits on the allowable control surface deflections, no knowledge of the flexible coordinates in the dynamic inversion process, and both control surface deflection limits and no knowledge of flexible coordinates.

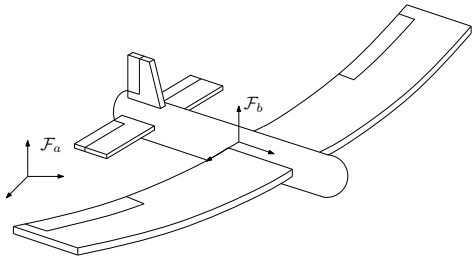

Fig. 1. Visualization of a flexible aircraft with body frame $\mathcal{F}_b$ and inertial frame $\mathcal{F}_a$.

The remainder of this paper proceeds as follows. A presentation of the equations of motion of a flexible aircraft is included in Section 2. Section 3 includes the dynamic inversion framework used to control the attitude of a flexible

2405-8963
Peer review under responsibility of International Federation of Automatic Control.
10.1016/j.ifacol.2016.09.058

aircraft. Numerical simulations of the proposed controller and variations of the proposed controller are presented in Section 4, followed by concluding remarks in Section 5.

2. DYNAMIC MODEL

Consider the flexible aircraft shown in Fig. 3 whose equations of motion are

$$\mathbf{M}\dot{\boldsymbol{\nu}} + \mathbf{D}\dot{\mathbf{q}} + \mathbf{K}\mathbf{q} + \mathbf{f}_{\text{non}}(\mathbf{q}, \boldsymbol{\nu}) = \hat{\mathbf{B}} \begin{bmatrix} \boldsymbol{\tau} \\ T \end{bmatrix}, \tag{1}$$

where $\mathbf{q}^\mathsf{T} = \begin{bmatrix} \mathbf{r}_a^{cw\mathsf{T}} & \mathbf{c}^{ba\mathsf{T}} & \mathbf{q}_e^\mathsf{T} \end{bmatrix}$ are the generalized coordinates, $\boldsymbol{\nu}^\mathsf{T} = \begin{bmatrix} \dot{\mathbf{r}}_a^{cw\mathsf{T}} & \boldsymbol{\omega}_b^{ba\mathsf{T}} & \dot{\mathbf{q}}_e^\mathsf{T} \end{bmatrix}$ are the augmented generalized velocities, $\mathbf{r}_a^{cw}$ is the position of the center of mass of the aircraft relative to an unforced particle w expressed in the inertial frame $\mathcal{F}_a$, $\mathbf{c}^{ba}$ is a column matrix that contains the nine entries of the DCM that describes the attitude of the aircraft relative to $\mathcal{F}_a$, $\mathbf{q}_e$ are the elastic coordinates used to describe the elastic deformation of aircraft, $\boldsymbol{\omega}_b^{ba}$ is the angular velocity of the aircraft relative to $\mathcal{F}_a$ expressed in the body frame $\mathcal{F}_b$. The matrix $\mathbf{M} = \mathbf{M}^\mathsf{T} > 0$ is the mass matrix, $\mathbf{D}$ is the damping matrix, $\mathbf{K}$ is the stiffness matrix, $\mathbf{f}_{\text{non}}(\mathbf{q}, \boldsymbol{\nu})$ is a column matrix containing nonlinear terms including aerodynamic forces, $\hat{\mathbf{B}}$ is the matrix that distributes the inputs to the dynamic equations, $\boldsymbol{\tau}$ is the body torque input to the aircraft, and T is the thrust input to the aircraft that acts along the longitudinal axis of the aircraft. Although aircraft do not have actuators that can exert an arbitrary body torque, a body torque is considered as a input in this paper for simplicity and to allow for the use of a DCM-based attitude control law. The pitch, roll, and yaw moments can be mapped to the appropriate control surface deflections by solving a control allocation problem (Durham, 1994; Härkegård, 2004; Bodson, 2002). The equation of motion in (1) is rewritten in first-order state-space form as

$$\dot{\mathbf{x}} = \mathbf{f}(\mathbf{x}) + \mathbf{G}(\mathbf{x}) \begin{bmatrix} \boldsymbol{\tau} \\ T \end{bmatrix}, \tag{2}$$

where $\mathbf{x}^\mathsf{T} = \begin{bmatrix} \mathbf{q}^\mathsf{T} & \boldsymbol{\nu}^\mathsf{T} \end{bmatrix}$,

$$\mathbf{f}(\mathbf{x}) = \begin{bmatrix} \boldsymbol{\Gamma}\boldsymbol{\nu} \\ \mathbf{f}_r(\mathbf{x}) \\ \mathbf{f}_\omega(\mathbf{x}) \\ \mathbf{f}_e(\mathbf{x}) \end{bmatrix},$$

$$\mathbf{G}(\mathbf{x}) = \begin{bmatrix} \mathbf{0} & \mathbf{0} \\ \mathbf{G}_{r\tau}(\mathbf{x}) & \mathbf{G}_{rT}(\mathbf{x}) \\ \mathbf{G}_{\omega\tau}(\mathbf{x}) & \mathbf{G}_{\omega T}(\mathbf{x}) \\ \mathbf{G}_{e\tau}(\mathbf{x}) & \mathbf{G}_{eT}(\mathbf{x}) \end{bmatrix}, \tag{3}$$

$$\begin{bmatrix} \mathbf{f}_r(\mathbf{x}) \\ \mathbf{f}_\omega(\mathbf{x}) \\ \mathbf{f}_e(\mathbf{x}) \end{bmatrix} = -\mathbf{M}^{-1} \left(\mathbf{D}\dot{\mathbf{q}} + \mathbf{K}\mathbf{q} + \mathbf{f}_{\text{non}}(\mathbf{q}, \boldsymbol{\nu}) \right),$$

$$\begin{bmatrix} \mathbf{G}_{r\tau}(\mathbf{x}) & \mathbf{G}_{rT}(\mathbf{x}) \\ \mathbf{G}_{\omega\tau}(\mathbf{x}) & \mathbf{G}_{\omega T}(\mathbf{x}) \\ \mathbf{G}_{e\tau}(\mathbf{x}) & \mathbf{G}_{eT}(\mathbf{x}) \end{bmatrix} = \mathbf{M}^{-1}\hat{\mathbf{B}},$$

$$\boldsymbol{\Gamma} = \text{diag}\{\mathbf{1}, \boldsymbol{\Gamma}_b^{ba}, \mathbf{1}\},$$

and $\dot{\mathbf{c}}^{ba} = \boldsymbol{\Gamma}_b^{ba}\boldsymbol{\omega}_b^{ba}$. As shown in de Ruiter and Forbes (2014), the relationship $\dot{\mathbf{c}}^{ba} = \boldsymbol{\Gamma}_b^{ba}\boldsymbol{\omega}_b^{ba}$ stems from Poisson's equation, $\dot{\mathbf{C}}_{ba} = -\boldsymbol{\omega}_b^{ba^\times}\mathbf{C}_{ba}$, where

$$\mathbf{a}^\times = \begin{bmatrix} 0 & -a_3 & a_2 \\ a_3 & 0 & -a_1 \\ -a_2 & a_1 & 0 \end{bmatrix},$$

for $\mathbf{a} = [a_1 \ a_2 \ a_3]^\mathsf{T}$. Defining $\mathbf{C}_{ba}^\mathsf{T} = \begin{bmatrix} \mathbf{c}_1^{ba} & \mathbf{c}_2^{ba} & \mathbf{c}_3^{ba} \end{bmatrix}$ and $\mathbf{c}^{ba^\mathsf{T}} = \begin{bmatrix} \mathbf{c}_1^{ba^\mathsf{T}} & \mathbf{c}_2^{ba^\mathsf{T}} & \mathbf{c}_3^{ba^\mathsf{T}} \end{bmatrix}$ leads to

$$\boldsymbol{\Gamma}_b^{ba} = \begin{bmatrix} \mathbf{0} & -\mathbf{c}_3^{ba} & \mathbf{c}_2^{ba} \\ \mathbf{c}_3^{ba} & \mathbf{0} & -\mathbf{c}_3^{ba} \\ -\mathbf{c}_2^{ba} & \mathbf{c}_1^{ba} & \mathbf{0} \end{bmatrix}.$$

The matrices in (1) are further expressed as

$$\mathbf{M} = \begin{bmatrix} \mathbf{M}_{rr} & \mathbf{M}_{r\omega} & \mathbf{M}_{re} \\ \mathbf{M}_{r\omega}^\mathsf{T} & \mathbf{M}_{\omega\omega} & \mathbf{M}_{\omega e} \\ \mathbf{M}_{re}^\mathsf{T} & \mathbf{M}_{\omega e}^\mathsf{T} & \mathbf{M}_{ee} \end{bmatrix},$$

$$\mathbf{f}_{\text{non}} = \begin{bmatrix} \mathbf{f}_{\text{non},r} \\ \mathbf{f}_{\text{non},\omega} \\ \mathbf{f}_{\text{non},e} \end{bmatrix},$$

$$\mathbf{D} = \text{diag}\{\mathbf{0}, \mathbf{0}, \mathbf{D}_{ee}\},$$

$$\mathbf{K} = \text{diag}\{\mathbf{0}, \mathbf{0}, \mathbf{K}_{ee}\},$$

where $\mathbf{D}_{ee} = \mathbf{D}_{ee}^\mathsf{T} \geq 0$ and $\mathbf{K}_{ee} = \mathbf{K}_{ee}^\mathsf{T} \geq 0$.

3. DYNAMIC INVERSION

The output of the system is chosen to be

$$\mathbf{y} = \begin{bmatrix} \boldsymbol{\omega}_b^{ba} \\ \mathbf{1}_2^\mathsf{T}\mathbf{C}_{ba}\dot{\mathbf{r}}_a^{cw} \end{bmatrix}, \tag{4}$$

where $\mathbf{1}_2^\mathsf{T}\mathbf{C}_{ba}\dot{\mathbf{r}}_a^{cw}$ is the forward velocity of the aircraft, $\mathbf{1}_2^\mathsf{T} = [0 \ 1 \ 0]$, $\mathbf{C}_{ba}$ is the DCM that describes the attitude of $\mathcal{F}_b$ relative to $\mathcal{F}_a$, and $\dot{\mathbf{r}}_a^{cw}$ is the velocity of the aircraft's center of mass relative to an unforced particle expressed in $\mathcal{F}_a$. Taking the time derivative of (4) yields

$$\begin{aligned} \dot{\mathbf{y}} &= \begin{bmatrix} \dot{\boldsymbol{\omega}}_b^{ba} \\ \mathbf{1}_2^\mathsf{T}\left(-\boldsymbol{\omega}_b^{ba^\times}\mathbf{C}_{ba} + \ddot{\mathbf{r}}_a^{cw} \right) \end{bmatrix}, \\ &= \begin{bmatrix} \mathbf{f}_\omega(\mathbf{x}) + \mathbf{G}_{\omega\tau}(\mathbf{x})\boldsymbol{\tau} + \mathbf{G}_{\omega T}(\mathbf{x})T \\ \mathbf{1}_2^\mathsf{T}\left(-\boldsymbol{\omega}_b^{ba^\times}\mathbf{C}_{ba} + \mathbf{f}_r(\mathbf{x}) + \mathbf{G}_{r\tau}(\mathbf{x})\boldsymbol{\tau} + \mathbf{G}_{rT}(\mathbf{x})T \right) \end{bmatrix}, \\ &= \bar{\mathbf{f}}(\mathbf{x}) + \bar{\mathbf{G}}(\mathbf{x}) \begin{bmatrix} \boldsymbol{\tau} \\ T \end{bmatrix}. \end{aligned} \tag{5}$$

where

$$\bar{\mathbf{f}}(\mathbf{x}) = \begin{bmatrix} \mathbf{f}_\omega(\mathbf{x}) \\ \mathbf{1}_2^\mathsf{T}\left(-\boldsymbol{\omega}_b^{ba^\times}\mathbf{C}_{ba} + \mathbf{f}_r(\mathbf{x}) \right) \end{bmatrix},$$

$$\bar{\mathbf{G}}(\mathbf{x}) = \begin{bmatrix} \mathbf{G}_{\omega\tau}(\mathbf{x}) & \mathbf{G}_{\omega T}(\mathbf{x}) \\ \mathbf{1}_2^\mathsf{T}\mathbf{G}_{r\tau}(\mathbf{x}) & \mathbf{1}_2^\mathsf{T}\mathbf{G}_{rT}(\mathbf{x}) \end{bmatrix}.$$

Based on the structure of (5) the control input is chosen to be

$$\begin{bmatrix} \boldsymbol{\tau} \\ T \end{bmatrix} = \bar{\mathbf{G}}^{-1}(\mathbf{x}) \left(\bar{\mathbf{v}} - \bar{\mathbf{f}}(\mathbf{x}) \right), \tag{6}$$

which gives $\dot{\mathbf{y}} = \bar{\mathbf{v}}$, where $\bar{\mathbf{v}}^\mathsf{T} = \begin{bmatrix} \mathbf{v}_\omega^\mathsf{T} & \mathbf{v}_r^\mathsf{T} \end{bmatrix}$. Based on the chosen aircraft inputs and outputs, the matrix $\bar{\mathbf{G}}(\mathbf{x})$ will always be non singular. This may not always be true when using dynamic inversion with a different set of inputs and/or outputs. Substituting (6) into (5) gives

$$\dot{\boldsymbol{\omega}}_b^{ba} = \mathbf{v}_\omega, \tag{7}$$

$$\mathbf{1}_2^\mathsf{T}\left(-\boldsymbol{\omega}_b^{ba^\times}\mathbf{C}_{ba} + \ddot{\mathbf{r}}_a^{cw} \right) = \mathbf{v}_r. \tag{8}$$

Equation (7) represents the attitude dynamics, while (8) represents the forward velocity dynamics. A PID control law that incorporates the DCM directly is considered

for the attitude dynamics (Goodarzi et al., 2013). By using the DCM directly, the attitude control law is well-defined globally and avoids common issues, such as the kinematic singularities associated with Euler angles and the unwinding of quaternions (Chaturvedi et al., 2011). The control law is given by

$$\mathbf{v}_\omega = \mathbf{K}_p \left(\mathbf{C}_{bd} - \mathbf{C}_{bd}^\mathsf{T}\right)^\vee - \mathbf{K}_d \boldsymbol{\omega}_b^{ba} + \mathbf{K}_i \int_0^t \left(\left(\mathbf{C}_{bd} - \mathbf{C}_{bd}^\mathsf{T}\right)^\vee - k\boldsymbol{\omega}_b^{ba}\right) \mathrm{d}\tau, \quad (9)$$

where $\mathbf{K}_p = \mathrm{diag}\{k_{p,1}, k_{p,2}, k_{p,3}\}$, $\mathbf{K}_d = \mathrm{diag}\{k_{d,1}, k_{d,2}, k_{d,3}\}$, $\mathbf{K}_i = \mathrm{diag}\{k_{i,1}, k_{i,2}, k_{i,3}\}$, $0 < k_{p,j} < \infty$, $j = 1,2,3$, $0 < k_{d,j} < \infty$, $j = 1,2,3$, $0 < k_{i,j} < \infty$, $j = 1,2,3$, $0 < k < \infty$, $\mathbf{C}_{bd}$ is the DCM representing the relative attitude between $\mathcal{F}_b$ and a desired reference frame, $\mathcal{F}_d$, $\mathbf{C}_{bd} = \mathbf{C}_{ba}\mathbf{C}_{da}^\mathsf{T}$ is the attitude error, and $(\cdot)^\vee : \mathbb{R}^{n\times n} \to \mathbb{R}^n$ is the uncross operator defined as

$$\mathbf{A} = -\mathbf{A}^\mathsf{T} = \begin{bmatrix} 0 & -a_3 & a_2 \\ a_3 & 0 & -a_1 \\ -a_2 & a_1 & 0 \end{bmatrix},$$

where $\mathbf{A}^\vee = [a_1 \ a_2 \ a_3]^\mathsf{T}$. The PI airspeed controller used is given by

$$\mathbf{v}_r = -k_{p,r}\left(V - V_d\right) - k_{i,r}\int_0^t \left(V - V_d\right) \mathrm{d}\tau, \quad (10)$$

where V is the airspeed of the aircraft relative to the wind, V_d is the desired airspeed, $0 < k_{p,r} < \infty$ is the proportional control gain, and $0 < k_{i,r} < \infty$ is the integral control gain. PI control is used, rather than PID control, since a measurement of $\dot{V}$ is not readily available.

The control inputs $\boldsymbol{\tau}$ and T depend on the flexible coordinates, $\mathbf{q}_e$, and the flexible coordinate rates, $\dot{\mathbf{q}}_e$, which in practice are not measured. Without knowledge of these coordinates the dynamic inversion will not completely cancel out the system's nonlinear dynamics, which could have a significant impact on the closed-loop system's performance and stability. The simulations presented in Section 4 include a comparison of the closed-loop performance with knowledge of the flexible coordinates and flexible coordinate rates to the closed-loop performance without knowledge of these states.

4. NUMERICAL EXAMPLE

In this section a numerical example is presented to illustrate the benefits of using dynamic inversion for the control of a flexible aircraft. The aircraft used in simulation is a HALE vehicle characterized by its high aspect ratio and low structural weight. Examples of HALE aircraft include X-HALE (Cesnik et al., 2012), Helios (AeroVironment, Inc., 2015), and Phantom Eye (Boeing, 2015). The HALE aircraft used in simulation is based on the dynamic model of a kiteplane with flexible wings developed by Caverly and Forbes (2015) with the specifications listed in Table 1.

Although a body torque input is calculated in (6), this is converted to approximately equivalent control surface deflections (to make for a simpler interpretation of the results) by making some simplifying assumptions. It is assumed that a deflection of the ailerons provides a pure body torque about the longitudinal axis of the aircraft, a deflection of the elevators provides a body torque about the pitch axis of the aircraft, and a deflection of the rudder provides a body torque about the yaw axis of the aircraft. For the simulated aircraft, control surface deflections lead to a change in airfoil camber, which causes a change in the lift and drag produced by the airfoil.

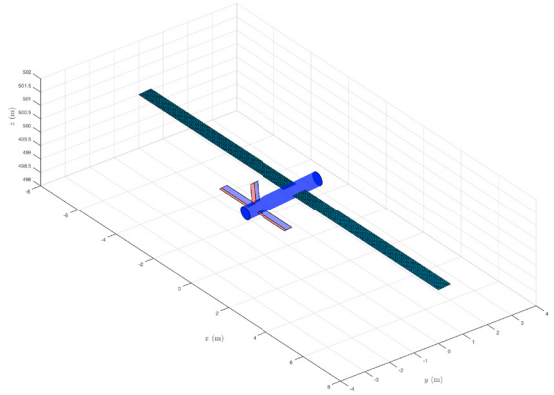

Fig. 3. Animation of the HALE aircraft used in the numerical simulations of Section 4.

Table 1. Main specifications of HALE aircraft used in the simulations of Section 4.

Property	Value
aircraft wingspan	16.5 m
aircraft length	4 m
aircraft mass	10 kg
wing airfoil	NACA 0012
wing chord length	0.5 m
wing aspect ratio	33
wing thickness	0.03 m
wing elastic modulus	40 GPa (carbon fiber)
horizontal stabilizer airfoil	NACA 0012
horizontal stabilizer chord length	0.5 m
horizontal stabilizer span	4.5 m
vertical stabilizer airfoil	NACA 0012
vertical stabilizer chord length	0.5 m
vertical stabilizer span	1 m

The first simulation is performed using the dynamic inversion control law of (6) with perfect knowledge of the model, including the flexible coordinates and flexible coordinate rates (denoted "dyn inv" in Fig. 2). This represents the ideal case, where all necessary model information and measurements are available. The chosen control gains are

$$\begin{aligned} k_{p,j} &= 5\,(\mathrm{rad/s^2}), \quad j = 1,2,3, \\ k_{d,j} &= 5\,(1/\mathrm{s}), \quad j = 1,2,3, \\ k_{i,j} &= 1\,(\mathrm{rad/s^3}), \quad j = 1,2,3, \\ k &= 1 \times 10^{-3}\,(\mathrm{s/rad}), \\ k_{p,r} &= 5\,(1/\mathrm{s}), \\ k_{i,r} &= 0.5\,(1/\mathrm{s^2}). \end{aligned}$$

The control gains are tuned to obtain short rise and settling times with little overshoot in the Euler angle and forward velocity responses. Different response characteristics can be obtained by different tuning of the control

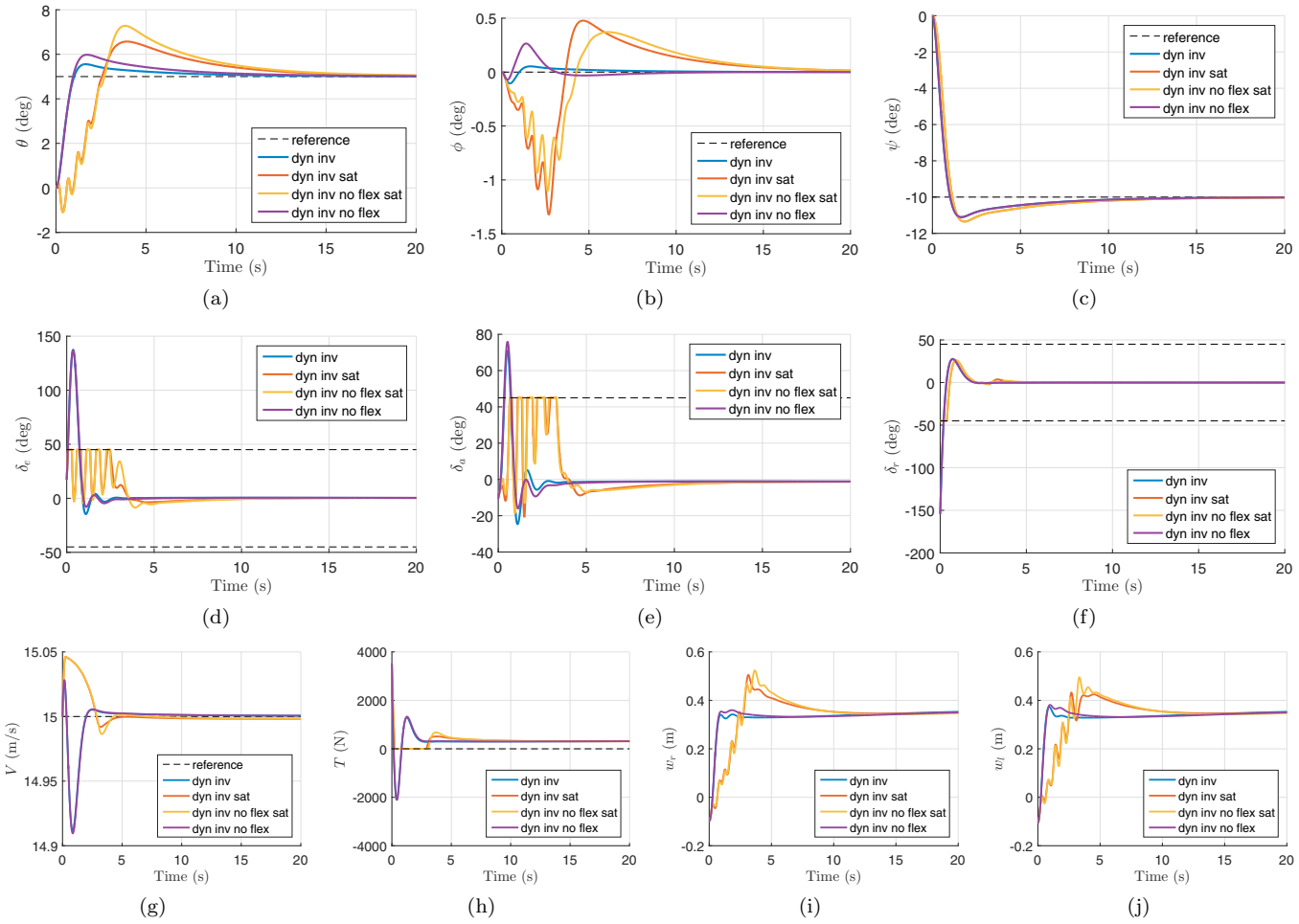

Fig. 2. Closed-loop system response plots of (a) pitch angle θ, (b) roll angle ϕ, (c) yaw angle ψ, (d) elevator deflection δ_e, (e) aileron deflection δ_a, (f) rudder deflection δ_r, (g) airspeed V, (h) thrust T, (i) right leading-edge wingtip deflection w_r, and (j) left leading-edge wingtip deflection w_l. The dotted lines in (d), (e), (f), and (h) represent the control limits used when actuator saturation is considered.

gains. The following simulations use the same control gains without any retuning, in order to make a fair comparison to the results of the first simulation.

The second simulation is performed using the same control law with knowledge of the flexible coordinates and flexible coordinate rates, but with saturation limits on the allowable control surface deflections set to ± 45 deg and minimum thrust of 0 N (denoted "dyn inv sat" in Fig. 2). The chosen limits do not reflect the maximum control surface deflections of any particular aircraft, but are simply chosen to demonstrate the effect of control constraints.

The third simulation is performed with the control law of (6) assuming knowledge of the rigid aircraft dynamics, but no knowledge of the flexible coordinates and flexible coordinate rates and the same saturation limits from the previous simulation (denoted "dyn inv no flex sat" in Fig. 2). This means that any terms involving $\mathbf{q}_e$ or $\dot{\mathbf{q}}_e$ in (6) are omitted in the dynamic inversion process.

The final simulation is also performed without knowledge of the flexible states, but no saturation limits (denoted "dyn inv no flex" in Fig. 2).

The results of the four simulations are presented in Fig. 2. In particular the closed-loop responses of the pitch angle θ, roll angle ϕ, yaw angle ψ, elevator deflection δ_e, aileron deflection δ_a, rudder deflection δ_r, airspeed V, thrust T, right leading-edge wingtip deflection w_r, and left leading-edge wingtip deflection w_l are included.

As expected, the simulation with perfect dynamic inversion exhibits excellent performance, as the desired aircraft attitude and airspeed are attained fairly quickly without any steady-state error. Unfortunately, the control surface deflections used to achieve this performance are unrealistic. The controller without knowledge of the flexible states and no saturation ("dyn inv no flex") performs similarly to the ideal controller with a slightly slower response. Both controllers that include saturation induce some vibrations, but ultimately stabilize the aircraft. Even with the controllers that include saturation, the controller that has knowledge of the flexible states outperforms the one that does not.

5. CONCLUSIONS

A dynamic inversion control algorithm for the attitude and airspeed control of a flexible aircraft was presented in this

paper. The angular velocity and forward velocity equations of motion are inverted and a synthetic input is chosen using a DCM-based PID attitude control law and a PI airspeed control law. The effectiveness of the proposed dynamic inversion controller is demonstrated in simulation, and is compared to slightly more realistic variations of the same controller. As anticipated, the idealistic proposed dynamic inversion controller outperforms the other more realistic controllers, but the other controllers still produce reasonable results.

Future work will investigate the use of an extended Kalman filter (EKF) to estimate the flexible states of the aircraft for use in the dynamic inversion control law. This would allow for the practical implementation of the dynamic inversion control law of (6) with the inclusion of flexible states, which could potentially lead to improved performance, as seen in the closed-loop response of the ideal controller in Section 4.

Additional future work will consider control surface deflections as the aircraft's inputs. This will likely be a fly-by-wire flexible aircraft, where each aileron and each elevator can be operated independently. This would increase the number of system inputs and could possibly lead to improved closed-loop performance and stability properties. The addition of wing-based actuators (e.g., piezo-electric materials, control moment gyros, etc.) may be investigated to allow for more control authority over the closed-loop response of the flexible coordinates.

REFERENCES

AeroVironment, Inc. (2015). Helios (UAV): UAS Advanced Development Center. URL `https://www.avinc.com/uas/adc/helios/`.

Bodson, M. (2002). Evaluation of optimization methods for control allocation. *Journal of Guidance, Control, and Dynamics*, 25(4), 703–711.

Boeing (2015). Boeing: Phantom Eye. URL `http://www.boeing.com/defense/phantom-eye/`.

Caverly, R.J. and Forbes, J.R. (2015). Dynamic modeling, trajectory optimization, and control of a flexible kiteplane. *IEEE Transactions on Control Systems Technology*. Under Review.

Cesnik, C.E.S., Senatore, P.J., Su, W., Atkins, E.M., and Shearer, C.M. (2012). X-HALE: A very flexible unmanned aerial vehicle for nonlinear aeroelastic tests. *AIAA Journal*, 50(12), 2820–2833.

Chaturvedi, N.A., Sanyal, A.K., and McClamroch, N.H. (2011). Rigid-body attitude control. *IEEE Control Systems Magazine*, 31(3), 30–51.

de Ruiter, A.H.J. and Forbes, J.R. (2014). General identities for parameterizations of SO(3) with applications. *J. Appl. Mech.*, 81(7), 071007.

Dillsaver, M.J., Cesnik, C.E.S., and Kolmanovsky, I.V. (2013). Trajectory control of very flexible aircraft with gust disturbance. In *AIAA Atmospheric Flight Mechanics (AFM) Conference*. Boston, MA.

Durham, W.C. (1994). Constrained control allocation: Three-moment problem. *Journal of Guidance, Control, and Dynamics*, 17(2), 330–336.

Enns, D., Bugajski, D., Hendrick, R., and Stein, G. (1994). Dynamic inversion: An evolving methodology for flight control design. *International Journal of Control*, 59(1), 71–91.

Goodarzi, F., Lee, D., and Lee, T. (2013). Geometric nonlinear PID control of a quadrotor UAV on SE(3). In *Proceedings of the European Control Conference*, 3845–3850.

Gregory, I.M. (2001). Stability result for dynamic inversion devised to control large flexible aircraft. In *AIAA Guidance, Navigation, and Control Conference*, 4282.

Härkegård, O. (2004). Dynamic control allocation using constrained quadratic programming. *Journal of Guidance, Control, and Dynamics*, 27(6), 1028–1034.

Hovakimyan, N., Lavretsky, E., and Sasane, A.J. (2005). Dynamic inversion for nonaffine-in-control systems via time-scale separation: Part i. In *Proceedings of the American Control Conference*, 3542–3547. Portland, OR.

Malekzadeh, M., Naghash, A., and Talebi, H.A. (2010). Control of flexible spacecraft using dynamic inversion and μ-synthesis. *Journal of Vibration and Control*, 17(13), 1938–1951.

Patil, M.J., Hodges, D.H., and Cesnik, C.E.S. (1999). Nonlinear aeroelasticity and flight dynamics of high-altitude long-endurance aircraft. In *Structures, Structural Dyanmics, and Materials Conference*.

Sastry, S.S. and Isidori, A. (1989). Adaptive control of linearizable systems. *IEEE Transactions on Automatic Control*, 34(11), 1123–1131.

Tafazoli, S. and Khorasani, K. (2004). Nonlinear control and stability analysis of spacecraft attitude recovery. *IEEE Transactions on Aerospace and Electronic Systems*, 42(3), 825–845.

Tuzcu, I., Marzocca, P., Cestino, E., Romeo, G., and Frulla, G. (2007). Stability and control of a high-altitude, long endurance UAV. *Journal of Guidance, Control, and Dynamics*, 30(3), 713–721.